Emergence of an Antigenically Drifted and Reassorted Influenza B Virus at the end of the 2024-25 Influenza Season

Elgin Akin[a], David A. Villafuerte[a,b], Anne P. Werner [a], Matthew Pinsley[a], Amary Fall[b], Omar Abdullah[b], Julie M. Norton[b], Richard E. Rothman[c], Katherine Z.J. Fenstermacher[c], Yu-Nong Gong [d,e,f], Eili Klein[g, h] , Heba H. Mostafa[b#], Andrew Pekosz[a, g#]

[a]Harry Feinstone Department of Molecular Microbiology and Immunology, Johns Hopkins Bloomberg School of Public Health, Baltimore, MD USA
[b]Department of Pathology, Johns Hopkins University School of Medicine, Baltimore, Maryland, USA
[c]Department of Emergency Medicine, Johns Hopkins University School of Medicine, Baltimore, Maryland, USA
[d]Research Center of Emerging Viral Infections, College of Medicine, Chang Gung University, Taoyuan, Taiwan;
[e]International Master Degree Program for Molecular Medicine in Emerging Viral Infections, College of Medicine, Chang Gung University, Taoyuan, Taiwan
[f]Department of Emergency Medicine, Keelung Chang Gung Memorial Hospital, Keelung, Taiwan
[g]Department of Emergency Medicine, Johns Hopkins School of Medicine, Baltimore, MD 21287, USA
[h]Center for Disease Dynamics, Economics, and Policy, Washington, DC 20005, USA.

Running Head: Phenotypic effects of IBV C.3 reassortant subclade

[#]Corresponding Authors:
Heba Mostafa, hmostaf2@jhmi.edu
Andrew Pekosz, apekosz1@jhu.edu

Abstract Word Count: 308
Body Word Count: 2590
References: 37
3 figures and 2 tables

Abstract

BACKGROUND

Influenza B virus is a significant contributor to annual total and severe cases of influenza, particularly in the young and elderly. Coupling whole virus genome sequencing with the monitoring of influenza cases allows for the identification of increased disease burden and the emergence of novel virus variants.

METHODS

Influenza B virus infected individuals were identified in the Johns Hopkins Health Systems network and whole IBV genome sequencing was performed. Phylogenetic analysis and sequence alignments were used to identify the IBV clades and novel virus mutations. The amount of neutralizing antibody activity specific to different IBV clades was measured.

RESULTS

Late in the 2024-25 Northern Hemisphere influenza season, a surge of IBV cases were identified. The IBV responsible for the surge, C.3re, was a clade C.3 virus that had reassorted with clade C.5.1 viruses and acquired a mutation predicted to mask a key neutralizing antibody epitope on the hemagglutinin protein. The neuramindase gene contained mutations predicted to reduce neutralizing antibody binding and potentially alter oseltamivir sensitivity. The C.3re viruses preferentially infected children but showed no significant increase in disease severity. The C.3re viruses were poorly neutralized by pre and post influenza vaccination serum.

CONCLUSIONS

The C.3re IBV genotype that emerged in late in the 2024-25 influenza season is antigenically mismatched with current circulating IBVs and the IBV vaccine strains chosen for the 2025 Southern Hemisphere and 2024-25 Northern Hemisphere season. This may result in lower vaccine efficacy increases in IBV cases in upcoming influenza seasons.

INTRODUCTION

Seasonal epidemics of influenza are caused by influenza A and B viruses, resulting in an estimated 250,000 to 500,000 global deaths annually [1,2]. Influenza B virus (IBV) can predominate in certain seasons; notably, during the 2019–2020 Northern Hemisphere season, IBVs accounted for 61% of pediatric influenza deaths despite comprising only 41% of overall infections[3,4]. IBVs are defined by clade designations resulting from genetic differences in the hemagglutinin (HA) gene, which shapes both antigenic identity and viral fitness [5]. When mutations disrupt epitopes recognized by antiviral antibodies, antigenically drifted viruses can emerge and become dominant in the population [6]. Epitopes can also be masked by the addition of post translational modifications such as N-linked glycans which can prevent antibodies from binding to epitopes through steric hindrance [7,8]. Mutations in HA can impact HA receptor binding [9–12], while mutations in other gene segments can alter replication efficiency [13–15], innate immune evasion[14–1616–18] or transmissibility. The segmented nature of the genome also allows for reassortment between genetically distinct IBV viruses, resulting in progeny viruses that have acquired new constellations of mutations that can affect antigenic structure, in virus replication or antiviral drug sensitivity [19–22].

IBV subclade C.5.1 has dominated North American circulation in recent seasons, while C.3 represented a minor component accounting for ≤5% of sequenced IBV viruses. The 2024-25 influenza season in the U.S. was marked by limited spread of IBV, with only 5% of sequence confirmed infections attributed to IBV. The season was dominated by clades C.5.7, C.5.6 and C.5.1 until early spring, when there was a surge of IBV cases caused by clade C.3 viruses. We undertook an analysis of the late season IBV cases to identify the cause of the surge.

METHODS

Cell Culture

Madin-Darby canine kidney (MDCK) cells (provided by Dr. Robert A. Lamb, Northwestern University), MDCK-SIAT-1 cells (provided by Dr. Scott Hensley, University of Pennsylvania) and MDCK-SIAT-1-TMPRSSII cells (provided by Dr. Jesse Bloom, Fred Hutchinson Cancer Center) were maintained in complete medium (CM) consisting of Dulbecco's Modified Eagle Medium (DMEM) supplemented with 10% fetal bovine serum, 100 units/ml penicillin/streptomycin (Life

Technologies) and 2 mM Glutamax (Gibco) at 37 °C and 5% CO2. Human nasal epithelial cells (hNEC) (PromoCell) were cultivated as previously described [8].

Virus Isolation on Human Nasal Epithelial Cells *(hNECs) and TMPRSSII cells*

Nasopharyngeal swabs or nasal washes from individuals who were influenza A positive were used for virus isolation on MDCK-SIAT-TMPRSS2 cells or human nasal epithelial cell (hNEC) cultures as described previously [8,37]. The MDCK-SIAT-TMPRSS2 cells were cultured at 37°C with 5% CO2 in complete medium (CM) consisting of Dulbecco's Modified Eagle Medium (DMEM) supplemented with 10% fetal bovine serum, 100 units/ml penicillin/streptomycin (Life Technologies, Carlsbad, CA, USA) and 2 mM Glutamax (Gibco, Waltham, MA, USA). For virus isolation, the cells were grown in 96 well dishes, washed twice with 300ul of phosphate buffered saline (PBS) and 50-90 µl of specimen was added to the cells and incubated for two hours at 37°C. The supernatant was then aspirated and cells were washed twice with 300 µl of PBS, then incubated at 33°C for three, five, and seven days in 100 µl of infection media (DMEM supplemented with 0.3% BSA (Sigma-Aldrich, St. Louis, MO, USA), 100 units/ml pen/strep, 2 mM Glutamax (Thermo-Fisher, Waltham, MA, USA). TCID50 was performed on collected supernatants and virus seed stocks were made from the collected media when virus was detected at concentrations greater than 10^4 TCID50/mL.

Virus Stock Preparation

A T75 flask of confluent MDCK-SIAT-1 cells was infected at an MOI of 0.01. Working stocks for each vaccine strain or clinical isolate were generated by infecting a T75 flask of MDCK-SIAT-1 cells at an MOI of 0.001 for one hour at room temperature while rocking. The inoculum was removed, and cells were placed in a 33 °C incubator and monitored daily for CPE. Working stock was harvested between 3 and 5 days later, when CPE was seen in 75–80% of the cells. Harvested media were centrifuged at 400× *g* for 10 min at 8 °C to remove cell debris, and the resulting supernatant was aliquoted into 500 µL and stored at −80 °C infectious virus quantity of working stocks was determined using TCID-50 assay. Seed and working stocks of the egg-adapted vaccine strains of IBV were grown directly in MDCK-SIAT-1 cells as described above. IBV vaccine strains were kindly provided by Johns Steel, US Centers for Disease Control (CDC).

Tissue Culture Infectious Dose 50 ($TCID_{50}$) Assay

MDCK-SIAT-1 cells were seeded in a 96-well plate 2 days before assay and grown to 100% confluence. Cells were washed twice with PBS+ then 180 µL of IM was added to

each well. Ten-fold serial dilutions of virus from 10^{-1} to 10^{-7} were created and then 20 µL of the virus dilution was added to the MDCK-SIAT-1 cells. Cells were incubated for 6 days at 33 °C then fixed with 2% formaldehyde. After fixing, cells were stained with Naphthol Blue Black, washed and virus titer was calculated using the Reed and Muench method.

Phylogenetic Reconstruction

Nextclade was used to call clade and subclade designation (https://github.com/influenza-clade-nomenclature/seasonal_B-Vic_HA/blob/main/subclades/C.3.yml; last accessed July 6th, 2025).

Ethical considerations and human subject approval

The Johns Hopkins Institutional Review Board has approved this work. The research was performed under protocols IRB00091667 and IRB00331396. Genomes are available in the Global Initiative on Sharing All Influenza Data (GISAID) database. Accession numbers available in **Supplementary table 1**. Serologic samples for this study were obtained from healthcare workers (HCWs) recruited from the Johns Hopkins Centers for Influenza Research and Response (JH-CEIRR) during the annual Johns Hopkins Health System (JHHS) employee influenza vaccination campaign in the Fall of 2024. Serum was collected from subjects at the time of vaccination and approximately 28 days later. Virus was isolated for this study from deidentified IBV positive nasal swabs under the JHU School of Medicine Institutional Review Board approved protocol, IRB00288258.

Acute Infection Study Population

Standard-of-care diagnostic influenza testing was conducted at the JHHS. Detection of influenza virus was performed with either the Cepheid Xpert Xpress SARS-CoV-2/Flu/respiratory syncytial virus test (Sunnyvale, CA, USA) or the ePlex RP/RP2 respiratory panels (Roche Diagnostics, Indianapolis, IN, USA). The Xpert Xpress assay targets the matrix the M and NSP segments for IBV. Clinical samples were collected between December 2024 and April 2025, and corresponding clinical and demographic metadata were extracted in bulk through JHHS electronic medical charts.

Nucleic acid extraction and whole genome amplification

Nucleic acid was extracted using the Chemagic Viral RNA/DNA Kit following the manufacturer's instructions (Revvity, Waltham, MA, USA). The whole genomes of IBV were amplified using Invitrogen Supercript III (Waltham, MA, USA) and universal IBV primer cocktail. Library preparation was performed with NEBNext Artic SARS-CoV-2 Companion Kit (New England Biolabs, Ipswich, MA, USA), and sequencing was performed following manufacturer's instructions, using R10.4.1 flow cells on a GridION (Oxford Nanopore Technologies, Oxford, UK).

Virus genome assembly

Fastq files were demultiplexed using the artic_guppyplex tool (Artic version 1.2.2). Nucleotide sequence assembly was performed using the default settings of the FLU module of the Iterative Refinement Meta-Assembler (IRMA version 1.0.2) which include a minimum average quality score of 24 and a site depth of 100. The alignment of genomes and reference sequences, downloaded from GISAID, was performed using the built-in alignment tool in Nextclade. Quality control scores for sequences were assigned using the built-in pipeline available in Nextclade. Sequences with scores of 30 and above were excluded from sequence analysis.

Phylogenetic Analysis of Influenza B Segments and Concatenated Genomes

Whole genome sequences were obtained from GISAID or generated at Johns Hopkins Hospital (Table S5). All scripts used for phylogenetic reconstruction are publicly available at https://github.com/elginakin/influenzab_c.3.

Serum Neutralization Assay

Serum samples used for this analysis originated from JHHS healthcare workers recruited from the Johns Hopkins Center of Excellence for Influenza Research and Response (JH-CEIRR) during the Fall 2024 influenza vaccination campaign. Serum samples collected at the time of vaccination or 28 days post vaccination were first treated (1:3 ratio serum to enzyme) with Receptor Destroying Enzyme (Denka-Seiken, Tokyo, Japan) and incubated overnight at 37 °C followed by inactivation at 57 °C for 35 min. Serum was diluted 2-fold in IM (Dulbecco modified Eagle medium (Sigma), with 10% penicillin/streptomycin (Gibco), 10% L-glutamine (Gibco), 0.5% BSA (Sigma), and 5 µg/mL of N-acetyl trypsin (Sigma) at 37 °C and 5% CO_2) and 100 TCID50 was added for a one-hour incubation at room temperature. Serum Sample/Virus was used to infect a confluent layer of MDCK-SIAT-1 cells. The inoculums were removed after 24 hours, IM supplemented with 2.5µg/mL N-acetyl Trypsin was replaced, and cells were incubated

for 96 hours at 37°C. Plates were fixed and stained as described previously[16]. The Neutralizing Antibody titer was calculated using the highest serum dilution that led to greater than 50% CPE.

Statistical analyses

Statistical analyses were performed in R (4.3.2) or Graphpad Prism (10.4.2). Time to the most recent common ancestor estimates and confidence intervals were performed using Baltic.

Data availability

The datasets used and/or analyzed during the current study are available through the Johns Hopkins Research Data Repository at **[TODO: INSERT DOI WHEN RELEASED]**.

RESULTS

Replacement of the Influenza B virus V1A.3a.2 subclade C.5.1 with C.3 in the 2024-25 season

Within the JHHS, 15% (894/5365) of influenza-positive patients were infected with influenza B virus (IBV) in the 2024-25 season **(Figure 1A).** IBV cases rose sharply from 65 total cases in February to 372 and 400 cases in March and April respectively **(Figure 1A and Table S1).** A subset of IBV+ specimens were subject to long-read whole genome sequencing and 58.5% belonged to the C.3 subclade **(Figure 1B, Table 1)**. Subclade C.5.6 was detected at 22.3% and the formerly dominant 2023-24 subclade C.5.1 at 11.5% **(Table 1)**. C.5.7 and the parental C.5 subclades were detected in comparatively low abundance at 3.8% and 3.1%, respectively. Nationally, the percentage of C.3 infections was much lower than what was observed in the state of Maryland (18.3 versus 58.5%, **Table 2; Figure S1**)

2024–25 C.3 strains infect a younger population compared to C.5 subclade lineages but do not impact clinical symptoms or outcomes

A subset of 113 patients with complete IBV genome sequences (≥98% coverage across all eight segments) were used to compare clinical and demographic information **(Figure S2)** between C.3 (n=67) or C.5.X subclade (C.5.1, C.5.6, and C.5.7; n=46) infections. The median age of patients infected with C.3 viruses was 8 years**,** significantly younger than those infected with C.5.X viruses (median 13 years) **(Figure 1A-B)**. Notably, 40.3% of C.3-infected individuals were between 6–11 years of age**,** compared to only 17.4% in the C.5.X group **(Figure 1C; Table S2)**.

The age range was also more restricted for C.3 (38 years) versus C.5.X (57 years). No other clinical or demographic factors differentiated C.3 from C.5.X infected individuals.

2024-25 C.3 strains have a reverted HA1:D197N and NA: 186 and V395I mutations

HA segment sequence alignments revealed that all the 2024-25 C.3 subclade contained an additional N-linked glycan motif (N-X-S/T) due to a D197N substitution which is absent in the vaccine strain (B/Austria/1359417/2024) and circulating C.5.X subclades **(Figure 1E and F).** Structural mapping of residue 197 onto the Influenza B virus hemagglutinin (PDB: 4FQM) revealed the site directly overlaps with the receptor binding site (RBS) and the 190-helix—critical regions for receptor attachment and neutralizing antibody recognition **(Figure 1G**).

All C.3 genomes encode a V395I and a K186R substitution (**Figure 1H**) in the NA gene - mutations that only appear together sporadically in IBV sequences until late 2024/early 2025 (**Figure 1I**). The V395I mutation is located on the solvent-exposed 380-helix—a known antigenic site accessible to neutralizing antibodies and the K186R mutation is located near the NA enzymatic active site and has been previously associated with reduced oseltamivir susceptibility when present in combination with 262T (**Figure 1J**) [23,24].

C.3 Subclade Viruses in 2024-25 Acquired Multiple Gene Segments from C.5.1 Lineages

Time-resolved maximum likelihood phylogenies were generated using complete genome sequences to further characterize 2025 C.3 virus genomes (**Supplemental Table 2)**. Concatenated genome phylogenies demonstrate that 2024–25 C.3 viruses (n=68) formed a highly divergent, monophyletic outgroup relative to previously circulating C.3 viruses **(Figure 2A).**

To determine the ancestry of individual genome segments, gene trees were constructed for all eight segments. In the HA phylogeny, 2024–25 sequences annotated as C.3 reassortants (C.3re) formed a monophyletic outgroup related to historical C.3 viruses (**Figure 2B**). In contrast, in the NA phylogeny, these same C.3re viruses clustered exclusively with C.5.1 sequences, sharing a most recent common ancestor with B/Michigan/UML372159450/2020 and showing no clustering with other C.3-derived NA segments (**Figure 2C**), indicating that all C.3re viruses acquired their NA segment from a C.5.1 lineage.

A similar analysis of the remaining 6 gene segments indicated that the PA, NP and NS segments were consistent with a C.5.1 ancestry **(Figure 2D and Supplemental Figure S3-S4)**, with the precise ancestor determination for the NS segment being less clear due to limited sequence divergence across C subclades and sparse surveillance of C.3 viruses over the past four years **(Supplemental Figures S5)**. A graphical summary of C.3re genome composition is shown in **Figure 2E,** indicating C.3re as a 4:4 reassortant virus.

2024-25 C.3re strains are antigenically drifted from circulating C.5.1 and the 2024-25 vaccine strain

Serum neutralizing antibody titers against the 2024–25 vaccine strain (B/Austria/1359417/2024; subclade C), a C.5.1 virus from the 2023–24 season (B/Baltimore/JH-547/2024), and a representative C.3re virus from 2024–25 (B/Baltimore/JH-1192/2025) were measured at the time of vaccination (day 0) and 28 days post-vaccination in a cohort of 50 individuals (**Table 2**). While both the vaccine and circulating C.5 clade viruses were recognized equivalently by pre and post vaccination sera, the C.3re viruses showed markedly reduced titers **(Figure 3A–B).** 84% of individuals (42/50) had no detectable neutralizing antibodies to C.3re at the time of vaccination and following vaccination, 78% (39/50) remained negative. Only one individual met the definition of seroconversion (≥4-fold NT_{50} increase) for C.3, while 19/50 and 18/50 individuals seroconverted for the vaccine and C.5.1 clade virus respectively **(Figure 3C)**. The mean increase in neutralization titer after vaccination rose 1.2 fold to the assay's limit of detection for C.3re (**Figure 3D**) while titers increased nearly 8-fold for the vaccine and 6.2-fold for the C.5.1 clade virus **(Table S4)**. These results indicate the C.3re viruses can evade preexisting population immunity (titers at time of vaccination) as well as seasonal influenza vaccine induced immunity (titers post vaccination).

C.3re Circulation Is Centered in the United States with Evidence of Global Dissemination

In July, 2025, global genomic surveillance data indicate that C.3re viruses were most prevalent in the United States, where they represent the majority of recent IBV detections (**Supplemental Figure 7A–B**). Notably, a single C.3re case was reported in the Southern Hemisphere—B/Tasmania/31/2025 (GISAID accession: EPI4411087)— at the beginning of the 2026 Southern Hemisphere influenza season.

DISCUSSION

During the 2024–25 influenza season, a reassorted and antigenically distinct IBV, designated C.3re, was identified that displaced the C.5.1 subclade lineage in Baltimore, MD. The reassorted C.3re preferentially infected younger individuals (median age 8 years), with 40.3% of cases occurring in children aged 6-11 years**.** This demographic shift may represent limited immunity to IBV C.3re in younger age groups, given the dominance of subclade C.5.X IBVs in recent years. In a cohort of 50 vaccinated healthcare workers, most of the individuals had no neutralizing antibody titers to C.3re either before or after influenza vaccination, indicating the C.3re escaped both preexisting population immunity and vaccine induced population immunity. The low level of serum neutralizing antibodies to C.3re but not to C.5.1 in our adult influenza vaccine population may also reflect that serum neutralizing antibody responses in the human population may be skewed to the C.5.1 HA protein 190 helix, and therefore an N-linked glycan that masks that epitope can eliminate a large portion of the serum neutralizing antibody response.

The IBV vaccine component in the 2024-25 northern hemisphere formulation was the subclade C virus B/Austria/1359417/2024 (clade V1A.3a.2), which has been used since 2022. The current interim vaccine effectiveness (VE) estimates are based on IBV clade C.5.X viruses that circulated early in the season and show 58% VE in Europe but too few IBV cases for an accurate assessment in the U.S. [25,26]. Nationally, IBV made up 17.2% of influenza positives tests (week ending in Jun 28, 2025)[27]. Ferret serum raised from egg-culture-adapted B/Austria/1359417/2024 recognized 96.6% of clinically IBV isolates by hemagglutination inhibition[28], but again, all these results were primarily obtained with C.5.X subclade IBVs[29]. Our results would predict that overall, VE against IBV will drop towards the end of the 2024-25 influenza season with the emergence of C.3re.

The addition of an N-linked glycan in the hemagglutinin (HA) receptor binding site (RBS) is a well-known determinant of epitope masking [7]. Furthermore, IBV HA Site 194-197 has been recognized as a highly plastic site with high rates of positive selection [30]. Acquisition of an N-linked glycan at this site in IBVs has been observed to impair antibody binding post-vaccination [31,32] and the loss of N-linked glycans has been associated with adaption of IBV to replication in embryonated chicken eggs, resulting in vaccines that generate antibodies with poor recognition of circulating, glycosylated IBV strains [33,34]. Since a 190 helix that lacks a N-linked glycosylation

has been present on circulating and vaccine strain IBVs since 2022, it is possible the human population has developed a serum neutralizing response skewed to this epitope.

Intra-subtype reassortment between human influenza viruses has been previously observed to increase disease severity while further diversifying the repertoire of influenza gene segment combinations [35,36]. Reassortment frequently occurs in IBV, potentially due to more rapid genetic diversification which allows for the detection of reassortment [19,20]. Here, phylogenetic analyses revealed that C.3re viruses acquired multiple internal gene segments from co-circulating C.5.1 viruses, including the C.5.1 NA segment which carries a V395I mutation that may confer escape from some NA binding antibodies.

This study has several limitations. First, our genomic dataset reflects sequencing efforts skewed to a single hospital system and may not fully capture community transmission dynamics. Broader population-based surveillance was limited, and global representation in publicly available databases such as GISAID remains uneven, potentially obscuring the true geographic distribution of C.3re viruses. Not all IBV positive cases underwent whole-genome sequencing, and thus clade assignments were available for only a subset of patients. Furthermore, time-scaled phylogenies relied on maximum likelihood methods rather than Bayesian inference, which may underestimate uncertainty in tMRCA estimates. Geospatial information for individual patients was unavailable, precluding assessment of within-city or regional transmission patterns.

The emergence of C.3re occurred after IBV vaccine strain selections were made for the 2025-26 Northern Hemisphere influenza vaccine and therefore, it was not available to be considered as a vaccine strain candidate [37]. This highlights the need to shorten the time between influenza vaccine strain selection and the initiation of the fall seasonal influenza vaccine campaign in order to fully identify and characterize late season virus variants and allow them to be considered as vaccine candidates.

Acknowledgments

This work was supported by National Institutes of Health (NIH) contract 75N93021C00045 Johns Hopkins Centers of Excellence in Influenza Research and Response, and NIH T32 AI007417. The authors thank the healthcare workers who enrolled and participated in the study. We are grateful for the efforts of the clinical coordination team at the Johns Hopkins Hospitals who collected samples.

EA's participation as a student in the 2025 Workshop on Molecular Evolution (MOLE) at the Marine Biological Laboratory in Woods Hole, MA provided important insight into constructing phylogenies and reassortment networks pivotal to this study. We thank the laboratories of Heba Mostafa and Andrew Pekosz for discussion of data and future directions.

References

1. Bedford T, Riley S, Barr IG, et al. Global circulation patterns of seasonal influenza viruses vary with antigenic drift. Nature 2015;523(7559):217–20.

2. Thompson WW, Weintraub E, Dhankhar P, et al. Estimates of US influenza-associated deaths made using four different methods. Influenza Other Respir Viruses 2009;3(1):37–49.

3. Dawood FS. Interim Estimates of 2019–20 Seasonal Influenza Vaccine Effectiveness — United States, February 2020. MMWR Morb Mortal Wkly Rep [Internet] 2020 [cited 2025 Jul 11];69. Available from: https://www.cdc.gov/mmwr/volumes/69/wr/mm6907a1.htm

4. Costa JC da, Siqueira MM, Brown D, et al. Vaccine Mismatches, Viral Circulation, and Clinical Severity Patterns of Influenza B Victoria and Yamagata Infections in Brazil over the Decade 2010-2020: A Statistical and Phylogeny-Trait Analyses. Viruses 2022;14(7):1477.

5. Ni F, Kondrashkina E, Qinghua Wang, Qinghua Wang, Wang Q. Structural basis for the divergent evolution of influenza B virus hemagglutinin. Virology 2013;446(1):112–22.

6. Rosu ME, Lexmond P, Bestebroer TM, et al. Substitutions near the HA receptor binding site explain the origin and major antigenic change of the B/Victoria and B/Yamagata lineages. Proc Natl Acad Sci 2022;119(42):e2211616119.

7. Sun X, Jayaraman A, Maniprasad P, et al. N-Linked Glycosylation of the Hemagglutinin Protein Influences Virulence and Antigenicity of the 1918 Pandemic and Seasonal H1N1 Influenza A Viruses. J Virol 2013;87(15):8756–66.

8. Das SR, Hensley SE, David A, et al. Fitness costs limit influenza A virus hemagglutinin glycosylation as an immune evasion strategy. Proc Natl Acad Sci 2011;108(51):E1417–22.

9. Swanson NJ, Marinho P, Dziedzic A, et al. 2019–2020 H1N1 clade A5a.1 viruses have better in vitro fitness compared with the co-circulating A5a.2 clade. Sci Rep 2023;13(1):10223.

10. Wang Y-F, Chang C-F, Chi C-Y, Wang H-C, Wang J-R, Su I-J. Characterization of glycan binding specificities of influenza B viruses with correlation with hemagglutinin genotypes and clinical features. J Med Virol 2012;84(4):679–85.

11. Nakagawa N, Kubota R, Maeda A, Okuno Y. Influenza B Virus Victoria Group with a New Glycosylation Site Was Epidemic in Japan in the 2002-2003 Season. J Clin Microbiol 2004;42(7):3295–7.

12. Lee JM, Huddleston J, Doud MB, et al. Deep mutational scanning of hemagglutinin helps predict evolutionary fates of human H3N2 influenza variants. Proc Natl Acad Sci 2018;115(35):E8276–85.

13. Bae J-Y, Lee I, Kim JI, et al. A Single Amino Acid in the Polymerase Acidic Protein Determines the Pathogenicity of Influenza B Viruses. J Virol 2018;92(13):e00259-18.

14. Canaday LM, Resnick JD, Liu H, et al. HA and M2 sequences alter the replication of 2013–16 H1 live attenuated influenza vaccine infection in human nasal epithelial cell cultures. Vaccine 2022;40(32):4544–53.

15. Liu H, Grantham ML, Pekosz A. Mutations in the Influenza A Virus M1 Protein Enhance Virus Budding To Complement Lethal Mutations in the M2 Cytoplasmic Tail. J Virol 2018;92(1):e00858-17.

16. Wilson JL, Akin E, Zhou R, et al. The Influenza B Virus Victoria and Yamagata Lineages Display Distinct Cell Tropism and Infection-Induced Host Gene Expression in Human Nasal Epithelial Cell Cultures. Viruses 2023;15(9):1956.

17. Rowe T, Fletcher A, Lange M, et al. Delay of innate immune responses following influenza B virus infection affects the development of a robust antibody response in ferrets. mBio 2025;16(2):e02361-24.

18. Rowe T, Davis W, Wentworth DE, Ross T. Differential interferon responses to influenza A and B viruses in primary ferret respiratory epithelial cells. J Virol 2024;98(2):e01494-23.

19. Dudas G, Bedford T, Lycett S, Rambaut A. Reassortment between Influenza B Lineages and the Emergence of a Coadapted PB1–PB2–HA Gene Complex. Mol Biol Evol 2015;32(1):162–72.

20. McCullers JA, Wang GC, He S, Webster RG. Reassortment and Insertion-Deletion Are Strategies for the Evolution of Influenza B Viruses in Nature. J Virol 1999;73(9):7343–8.

21. Langat P, Raghwani J, Dudas G, et al. Genome-wide evolutionary dynamics of influenza B viruses on a global scale. PLOS Pathog 2017;13(12):e1006749.

22. Virk RK, Jayakumar J, Mendenhall IH, et al. Divergent evolutionary trajectories of influenza B viruses underlie their contemporaneous epidemic activity. Proc Natl Acad Sci 2020;117(1):619–28.

23. Brown SK, Tseng Y-Y, Aziz A, Baz M, Barr IG. Characterization of influenza B viruses with reduced susceptibility to influenza neuraminidase inhibitors. Antiviral Res 2022;200:105280.

24. Madsen A, Dai Y-N, McMahon M, et al. Human Antibodies Targeting Influenza B Virus Neuraminidase Active Site Are Broadly Protective. Immunity 2020;53(4):852-863.e7.

25. Frutos AM, Cleary S, Reeves EL, et al. Interim Estimates of 2024-2025 Seasonal Influenza Vaccine Effectiveness - Four Vaccine Effectiveness Networks, United States, October 2024-February 2025. MMWR Morb Mortal Wkly Rep 2025;74(6):83–90.

26. Rose AM, Lucaccioni H, Marsh K, et al. Interim 2024/25 influenza vaccine effectiveness: eight European studies, September 2024 to January 2025. Eurosurveillance 2025;30(7):2500102.

27. National, Regional, and State Level Outpatient Illness and Viral Surveillance [Internet]. [cited 2025 Jul 8];Available from: https://gis.cdc.gov/grasp/fluview/fluportaldashboard.html

28. CDC. Weekly US Influenza Surveillance Report: Key Updates for Week 20, ending May 17, 2025 [Internet]. FluView. 2025 [cited 2025 Jul 8];Available from: https://www.cdc.gov/fluview/surveillance/2025-week-20.html

29. Ben Moussa M, Nwosu A, Schmidt K, et al. National Influenza Annual Report 2023–2024: A focus on influenza B and public health implications. Can Commun Dis Rep 50(11):393–9.

30. Shen J, Kirk BD, Ma J, Wang Q. Diversifying Selective Pressure on Influenza B Virus Hemagglutinin. J Med Virol 2009;81(1):114–24.

31. Nakagawa N, Kubota R, Maeda A, Okuno Y. Influenza B Virus Victoria Group with a New Glycosylation Site Was Epidemic in Japan in the 2002-2003 Season. J Clin Microbiol 2004;42(7):3295–7.

32. Gatherer D. Passage in egg culture is a major cause of apparent positive selection in influenza B hemagglutinin. J Med Virol 2010;82(1):123–7.

33. Wilson JL, Zhou R, Liu H, Rothman R, Fenstermacher KZ, Pekosz A. Antigenic alteration of 2017-2018 season influenza B vaccine by egg-culture adaption. Front Virol [Internet] 2022 [cited 2025 May 9];2. Available from: https://www.frontiersin.orghttps://www.frontiersin.org/journals/virology/articles/10.3389/fviro.2022.933440/full

34. Saito T, Nakaya Y, Suzuki T, et al. Antigenic alteration of influenza B virus associated with loss of a glycosylation site due to host-cell adaptation. J Med Virol 2004;74(2):336–43.

35. Liu H, Shaw-Saliba K, Westerbeck J, et al. Effect of human H3N2 influenza virus reassortment on influenza incidence and severity during the 2017–18 influenza season in the USA: a retrospective observational genomic analysis. Lancet Microbe [Internet]

2024 [cited 2024 Jul 20];0(0). Available from: https://www.thelancet.com/journals/lanmic/article/PIIS2666-5247(24)00067-3/fulltext

36. Goldstein EJ, Harvey WT, Wilkie GS, et al. Integrating patient and whole-genome sequencing data to provide insights into the epidemiology of seasonal influenza A(H3N2) viruses. Microb Genomics 2018;4(1):e000137.

37. Recommended composition of influenza virus vaccines for use in the 2025-2026 northern hemisphere influenza season [Internet]. [cited 2025 Jul 11];Available from: https://www.who.int/publications/m/item/recommended-composition-of-influenza-virus-vaccines-for-use-in-the-2025-2026-nh-influenza-season

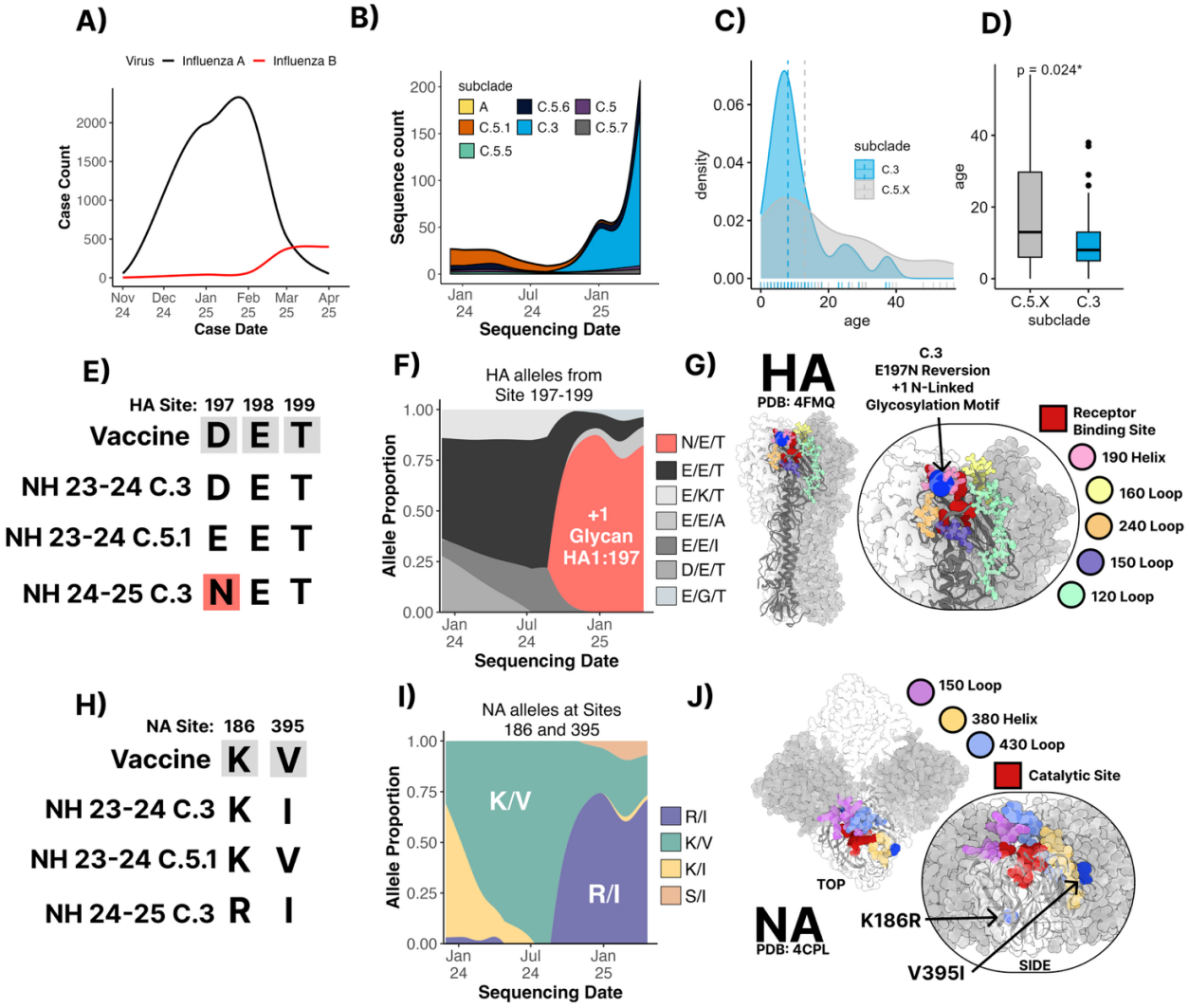

Figure 1

Figure 1. Emergence of Influenza B/Victoria C.3 subclade, acquisition of a novel glycosylation site, and age-related infection bias. **(A)** Weekly clinical case counts of influenza A (black) and B (red) reported from November 2024 to April 2025. **(B)** Longitudinal distribution of IBV B/Victoria HA subclades (colored by clade) based on sequencing data. **(C)** Kernel density estimate of patient age for sequences classified as C.3 (blue) or C.5.X (gray). Tick marks below each curve indicate individual ages. **(D)** Boxplot comparison of age distribution for C.3 versus C.5.X sequences (Wilcoxon test, p = 0.024). **(E)** Sequence alignment of HA (residues 197–199) protein motifs across the vaccine strain, parental C.5.1, C.3 and 2024-25 C.3 (B/Brisbane/08/2008 numbering). **(F)** The 2024–25 C.3 subclade acquired an N-linked glycosylation site at position 197 (N197), whereas C.5.1 retained the E197 motif. **(G)** Structural mapping of the D197N substitution onto the HA trimer (PDB: 4FMQ). The C.3-specific E197N mutation introduces an N-linked glycosylation site near the receptor binding domain. Key antigenic loops are annotated for reference. **(H)** NA sequence alignments reveal substitutions V395I and K186R. (I) the penetrance of mutations at positions 395 and 186 over time in IBV sequences. **(J)** NA structures showing the position of the V395I substitution in the 380-helix antigenic site and the K186R on the basal side of the NA

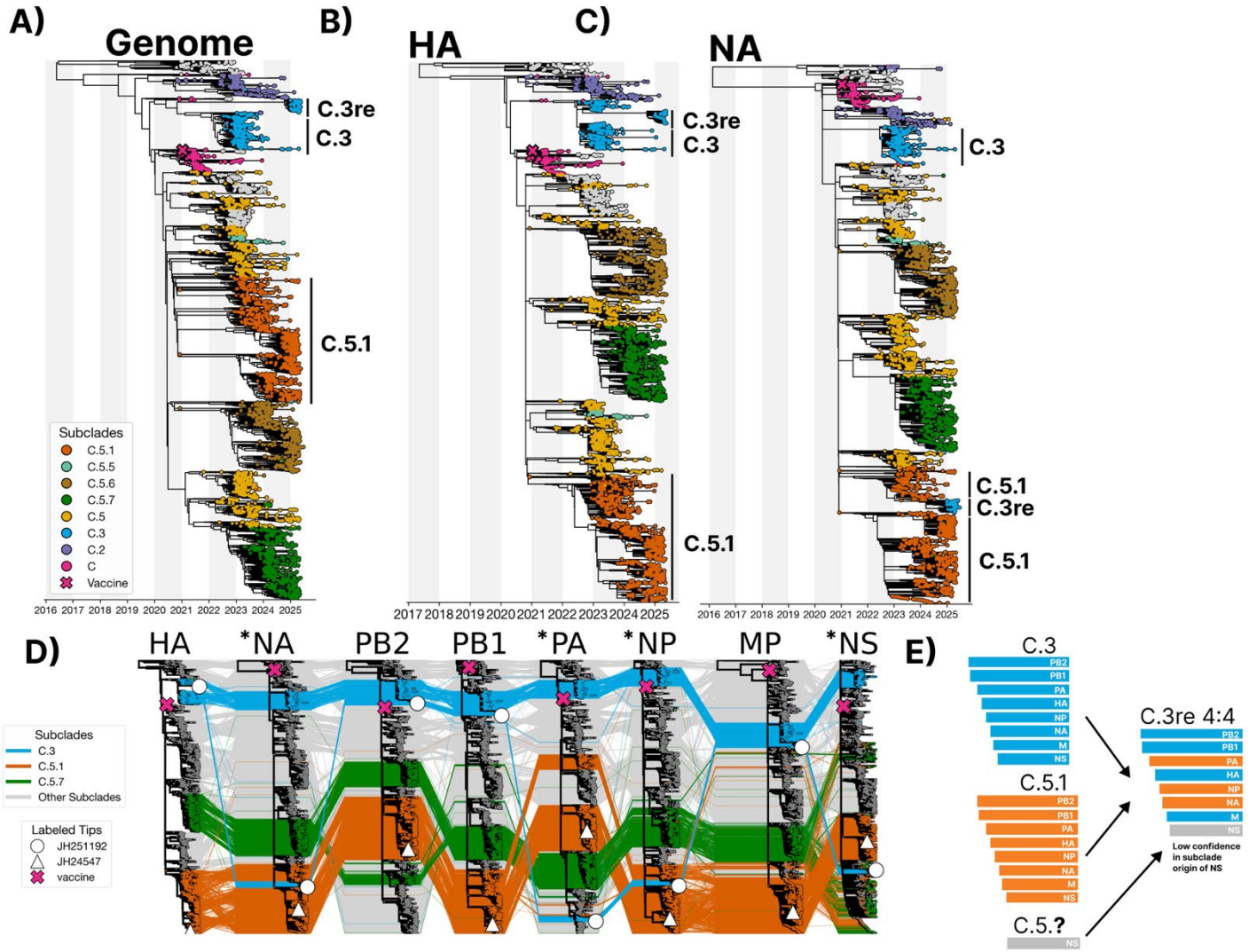

Figure 2

Figure 2 –2024-25 C.3 subclade viruses are 4:4 reassortment progeny with NA and internal segments derived from C.5.1 defined as C.3re.

(A) Maximum-likelihood phylogeny of concatenated genomes, HA **(B)** or NA **(C)** with leaves colored by subclade. Major subclades (C.3, C.5.1, C.5.5, C.5.6, C.5.7, C.5, C.2 and C) and annotated by color and the selected 2024-25 vaccine strain leaf (B/Austria/2021) annotated by shape. Branches were refined to inferred coalescent events using collection (reference) or sequencing date (JHH isolates) using augur refine. **(D)** 8 gene trees of each IBV segment interleaved and colored by HA subclade identity reveal a 4:4 reassortment with NA, PA, and NP clustering with the C.5.1 clade of each gene tree. The C.3re NS segment clusters in a diverged cluster containing strains with definitive C.5.1 and C.5.7 HA membership. Segments with the C.3 subclade which have originated from non-C.3 parental viruses are indicated with a " * ". **(E)** A cartoon schematic of inferred segment ancestry from each of the 8 gene trees in relation to the clinical specimen's HA subclade membership.

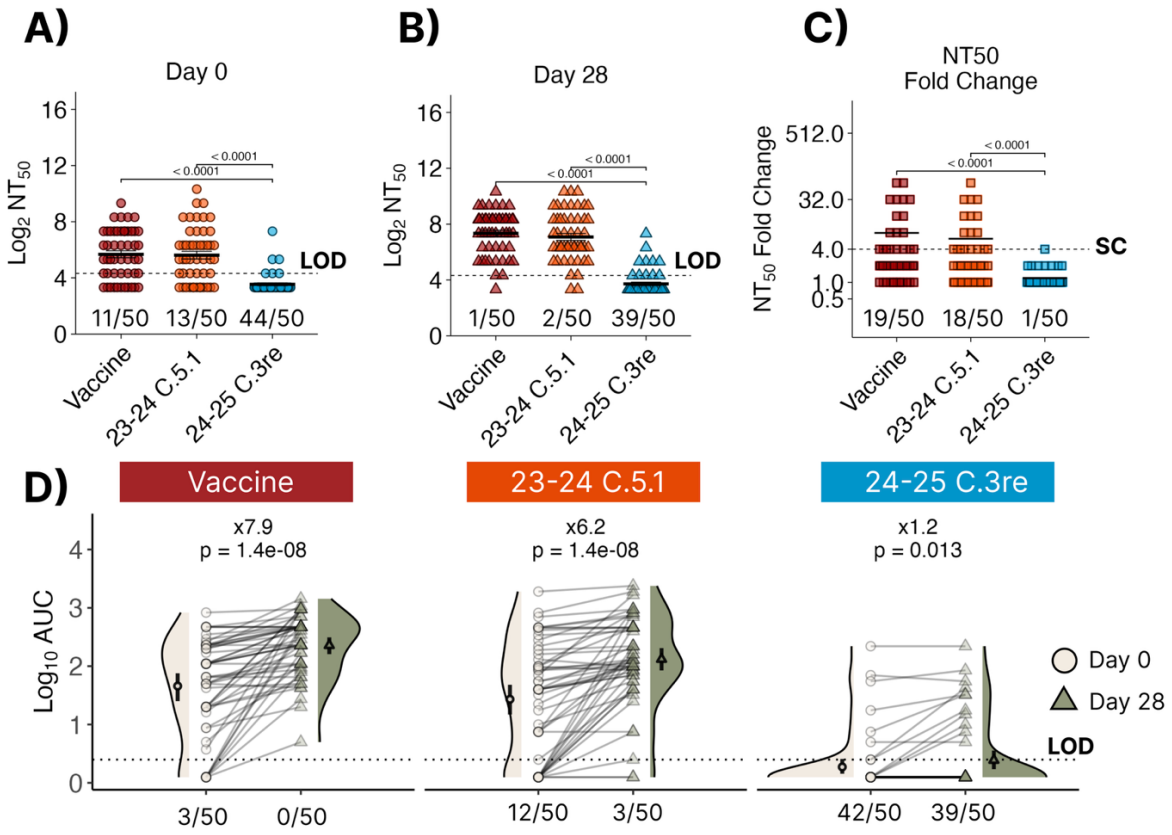

Figure 3

Figure 3. The C.3re subclade is antigenically drifted from both the vaccine strain B/Austria/1359417/2021 (subclade C) and the previously dominant C.5.1 subclade. The Johns Hopkins CEIRR Network influenza vaccine cohort consisted of 50 individuals receiving the 2023-24 trivalent Northern Hemisphere influenza vaccine. Serum neutralizing antibody titers (NT_{50}) with mean and standard error plotted **(A)** at the time of vaccination and **(B)** 28 days post vaccination against the 2023-24 B/Victoria vaccine strain (B/Austria/1359417/2021 subclade C) and a representative 2024-25 C.5.1 parental (B/Baltimore/JH-547/2024 subclade C.5.1) or a representative 2024-25 C.3re reassortment virus (B/Baltimore/JH-251192/2025). The number of seronegative individuals over the total number of individuals analyzed are shown under the datapoints for each virus. **(C)** NT_{50} fold change for day 0 to day 28 was used to determine seroconversion which was defined as a $NT_{50} \geq 4$. Individuals who seroconverted are shown as a fraction out of 50 beneath each data group. The dotted line represents the limit of detection (LOD), defined as the lowest value considered to be NT_{50} positive at the starting dilution of 1/20. No neutralizing activity is graphed as one-half the LOD. **(D)** Area under the curve (AUC) was calculated and used to show changes in titers at day 0 and day 28 post vaccination with an LOD set to 2.5. AUC fold change is shown above pairings. The number of seronegative individuals over the total number of individuals analyzed are shown under the datapoints for each virus. Statistical analysis within or between non-transformed NT_{50} or AUC timepoint values was performed using paired Wilcoxon tests with Bonferroni correction post-hoc. Adjusted p-values are shown above significantly different comparisons.

Table 1. Influenza B virus subclade sequence of down sampled GISAID submissions in Maryland vs North America

Subclade	C Maryland Count	North America Count	Maryland Percent	North America Percent
C.5.1	15	141	11.5	38.5
C.3	76	67	58.5	18.3
C.5.6	29	67	22.3	18.3
C.5.7	5	58	3.8	15.8
C.5	4	33	3.1	9.0

Table 2. 2024-25 JHJ-CEIRR Vaccine Cohort characteristics, demographics, and geometric mean titers for all assessments described. For qualitative data and co-morbidities, Fisher's exact test was used to generate p-values shown. For baseline and post-vaccination immunity readouts, adjusted p-values shown were calculated via Kruskal-Wallis nonparametric test with Bonferroni's correction for age analyses, and Dunn's test for multiple comparisons for sex analyses, both with Bonferroni's corrections. Bolded p-values area significant (i.e., $p < 0.05$).

	By sex				*By age group*				
	Female	**Male**	**Total**	**p-value**	**18-44**	**45-55**	**56-70**	**Total**	**p-value**
n (%)	25 (50.00)	25 (50.00)	50 (100.00)		24 (48.00)	12 (24.00)	14 (28.00)	50 (100.00)	
female, n (%)	25 (100.00)	0 (0.00)	25 (50.00)		10 (41.67)	9 (75.00)	6 (42.86)	25 (50.00)	
age in years, mean (SD)	44.44 (13.86)	44.44 (14.12)	44.44 (13.85)	1	31.71 (6.40)	50.25 (2.73)	61.29 (2.84)	44.44 (13.85)	-
BMI, mean (SD)	27.52 (5.75)	27.88 (5.61)	27.70 (5.63)	0.82	25.88 (5.36)	28.36 (4.30)	30.36 (6.26)	27.70 (5.63)	0.06
***Vaccine History*, n (%)**									
seasonal vaccine NH 2024-2025	25 (100.00)	25 (100.00)	50 (100.00)	>0.99	24 (100.00)	12 (100.00)	14 (100.00)	50 (100.00)	>0.99
no seasonal vaccine NH 2023-2024	1 (2.00)	3 (12.00)	4 (8.00)	0.61	3 (12.50)	1 (8.33)	0 (0.00)	4 (8.00)	0.45
no seasonal vaccine in any of previous 5 seasons	0 (0.00)	2 (8.00)	2 (4.00)	0.09	2 (8.33)	0 (0.00)	0 (0.00)	2 (4.00)	0.28
***Baseline Neutralization Titer 50%* , GMT (geom. SD)**									
V1A.3a.2 Subclade C - B/Austria/1359417/2021	50 (3.25)	53 (3.60)	51 (3.38)	0.867	60 (3.46)	32 (3.18)	59 (3.34)	51 (3.38)	0.296
V1A.3a.2 Subclade C.5.1 - B/Baltimore/JH-547/2024	43 (3.79)	56 (3.89)	49 (3.81)	0.453	34 (2.91)	57 (5.82)	84 (3.42)	49 (3.81)	0.118
V1A.3a.2 Subclade C.3re - B/Baltimore/JH-1192/2025	11 (1.32)	13 (1.88)	12 (1.63)	0.095	10 (1.00)	13 (2.23)	14 (1.69)	12 (1.63)	**0.006**
***Post-vaccination Neutralization Titer 50%* , GMT (geom. SD)**									
V1A.3a.2 Subclade C - B/Austria/1359417/2021	169 (3.10)	156 (2.91)	162 (2.97)	0.811	165 (2.92)	135 (3.77)	186 (2.58)	162 (2.97)	0.716
V1A.3a.2 Subclade C.5.1 - B/Baltimore/JH-547/2024	132 (2.86)	139 (4.06)	135 (3.41)	0.820	120 (3.06)	143 (4.11)	160 (3.68)	135 (3.41)	0.735
V1A.3a.2 Subclade C.3re - B/Baltimore/JH-1192/2025	11 (1.39)	16 (2.16)	13 (1.84)	0.075	11 (1.22)	14 (2.25)	18 (2.14)	13 (1.84)	**0.029**
***Baseline AUC*, GMT (geom. SD)**									
V1A.3a.2 Subclade C - B/Austria/1359417/2021	47 (5.96)	44 (8.00)	46 (6.81)	0.815	64 (5.21)	21 (7.94)	50 (8.61)	46 (6.81)	0.299
V1A.3a.2 Subclade C.5.1 - B/Baltimore/JH-547/2024	21 (9.85)	34 (9.83)	27 (9.73)	0.433	17 (8.19)	22 (17.18)	71 (6.37)	27 (9.73)	0.174
V1A.3a.2 Subclade C.3re - B/Baltimore/JH-1192/2025	2 (2.25)	2 (3.88)	2 (3.08)	0.129	1 (1.00)	2 (4.43)	3 (4.39)	2 (3.08)	**0.003**
***Post-vaccination AUC*, GMT (geom. SD)**									
V1A.3a.2 Subclade C - B/Austria/1359417/2021	228 (3.52)	227 (3.14)	227 (3.29)	0.883	238 (3.07)	160 (4.68)	284 (2.61)	227 (3.29)	0.582
V1A.3a.2 Subclade C.5.1 - B/Baltimore/JH-547/2024	125 (4.65)	139 (6.84)	132 (5.61)	0.741	104 (5.67)	156 (6.38)	173 (5.27)	132 (5.61)	0.501
V1A.3a.2 Subclade C.3re - B/Baltimore/JH-1192/2025	2 (2.65)	3 (5.14)	2 (3.95)	0.092	1 (1.84)	3 (5.20)	5 (5.87)	2 (3.95)	**0.032**
***Race*, n (%)**									
White	19 (76.00)	14 (56.00)	33 (66.00)	0.23	15 (62.50)	9 (75.00)	9 (64.29)	33 (66.00)	0.8
Hispanic/Latino	3 (15.79)	2 (14.29)	5 (15.15)	>0.99	3 (20.00)	2 (22.00)	0 (0.00)	5 (15.15)	0.48
Non-hispanic/Non-latino	16 (84.21)	12 (85.71)	28 (84.85)	>0.99	12 (80.00)	7 (78.78)	9 (100.00)	28 (84.85)	0.48
Black	3 (12.00)	7 (28.00)	10 (20.00)	0.29	5 (20.83)	1 (8.33)	4 (35.71)	10 (20.00)	0.53
Hispanic/Latino	0 (0.00)	0 (0.00)	0 (0.00)	-	0 (0.00)	0 (0.00)	0 (0.00)	0 (0.00)	-
Non-hispanic/Non-latino	3 (100.00)	7 (100.00)	10 (100.00)	-	5 (100.00)	1 (100.00)	4 (100.00)	10 (100.00)	-
Asian/Pacific Islander	1 (4.00)	2 (8.00)	3 (6.00)	>0.99	2 (8.33)	1 (8.33)	0 (0.00)	3 (6.00)	0.6
American Indian or Alaska Native	0 (0.00)	0 (0.00)	0 (0.00)	-	0 (0.00)	0 (0.00)	0 (0.00)	0 (0.00)	-
Other	2 (8.00)	2 (8.00)	4 (8.00)	>0.99	2 (8.33)	1 (8.33)	1 (7.14)	4 (8.00)	>0.99
N/A	0 (0.00)	0 (0.00)	0 (0.00)	-	0 (0.00)	0 (0.00)	0 (0.00)	0 (0.00)	-
***Comorbidities*, n (%)**									
Transplant recipient	0 (0.00)	0 (0.00)	0 (0.00)	-	0 (0.00)	0 (0.00)	0 (0.00)	0 (0.00)	-
Cancer (ongoing or remission)	2 (8.00)	0 (0.00)	2 (4.00)	0.49	0 (0.00)	1 (8.33)	1 (7.14)	2 (4.00)	0.27
Type II Diabetes	1 (4.00)	5 (20.00)	6 (12.00)	0.19	0 (0.00)	1 (8.33)	5 (35.71)	6 (12.00)	**0.004**
Autoimmune disease	0 (0.00)	0 (0.00)	0 (0.00)	-	0 (0.00)	0 (0.00)	0 (0.00)	0 (0.00)	-
Immunosuppressive medication	0 (0.00)	0 (0.00)	0 (0.00)	-	0 (0.00)	0 (0.00)	0 (0.00)	0 (0.00)	-
Methotrexate	-	-	0 (0.00)	-	-	-	-	0 (0.00)	-
Tacrolimus	-	-	0 (0.00)	-	-	-	-	0 (0.00)	-
Mycophenolate	-	-	0 (0.00)	-	-	-	-	0 (0.00)	-
Other	-	-	0 (0.00)	-	-	-	-	0 (0.00)	-
Hepatic disease	0 (0.00)	0 (0.00)	0 (0.00)	-	0 (0.00)	0 (0.00)	0 (0.00)	0 (0.00)	-
Renal disease	1 (4.00)	0 (0.00)	0 (0.00)	>0.99	1 (4.17)	0 (0.00)	0 (0.00)	1 (2.00)	>0.99
Cardiovascular disease	3 (12.00)	1 (4.00)	4 (8.00)	0.61	0 (0.00)	2 (16.67)	2 (14.29)	4 (8.00)	0.088
Chronic lung disease	3 (12.00)	1 (4.00)	4 (8.00)	0.61	2 (8.33)	2 (16.67)	0 (0.00)	4 (8.00)	0.25
Asthma	3 (100.00)	0 (0.00)	3 (60.00)	>0.99	1 (50.00)	2 (100.00)	0 (0.00)	3 (60.00)	>0.99
Other	0 (0.00)	1 (100.00)	1 (40.00)	>0.99	1 (50.00)	0 (0.00)	0 (0.00)	1 (40.00)	>0.99
Neurological disorder	0 (0.00)	0 (0.00)	0 (0.00)	-	0 (0.00)	0 (0.00)	0 (0.00)	0 (0.00)	-
Epilepsy	-	-	0 (0.00)	-	-	-	-	0 (0.00)	-
Stroke	-	-	0 (0.00)	-	-	-	-	0 (0.00)	-
Hematological disease	2 (8.00)	0 (0.00)	2 (4.00)	0.49	2 (8.33)	0 (0.00)	0 (0.00)	2 (4.00)	>0.99
Sickle cell disease	0 (0.00)	-	0 (0.00)	-	0 (0.00)	-	-	0 (0.00)	-
Anemia (non-sickle cell)	1 (50.00)	-	1 (2.00)	-	1 (50.00)	-	-	1 (2.00)	-
Other	1 (50.00)	-	1 (2.00)	-	1 (50.00)	-	-	1 (2.00)	-
Reproductive disease	7 (28.00)	0 (0.00)	7 (14.00)	**0.0003**	2 (8.33)	5 (41.67)	0 (0.00)	7 (14.00)	0.09
PCOS	1 (14.29)	-	1 (14.28)	-	1 (50.00)	0 (0.00)	-	1 (14.28)	-
Endometriosis	0 (0.00)	-	0 (0.00)	-	0 (0.00)	0 (0.00)	-	0 (0.00)	-
Primary ovarian insufficiency	0 (0.00)	-	0 (0.00)	-	0 (0.00)	0 (0.00)	-	0 (0.00)	-
Hysterectomy (full or partial)	4 (57.14)	-	4 (57.14)	**0.02**	0 (0.00)	4 (80.00)	-	4 (57.14)	**0.0046**
Other	2 (28.57)	-	2 (28.57)	>0.99	1 (50.00)	1 (20.00)	-	2 (28.57)	>0.99
Endocrine/Metabolic disease	3 (12.00)	1 (4.00)	4 (8.00)	0.35	1 (4.17)	1 (8.33)	2 (14.29)	4 (8.00)	0.42
Thyroid	3 (100.00)	1 (100.00)	4 (100.00)	0.61	1 (100.00)	1 (100.00)	2 (100.00)	4 (100.00)	0.68
Smoking history	3 (12.00)	2 (8.00)	5 (10.00)	>0.99	2 (8.33)	1 (8.33)	2 (14.29)	5 (10.00)	0.84
Current smoker?	1 (33.33)	1 (50.00)	2 (40.00)	>0.99	0 (0.00)	1 (100.00)	1 (50.00)	2 (40.00)	0.58
Past smoker?	2 (66.67)	1 (50.00)	3 (60.00)	>0.99	2 (100.00)	0 (0.00)	1 (50.00)	3 (60.00)	0.58

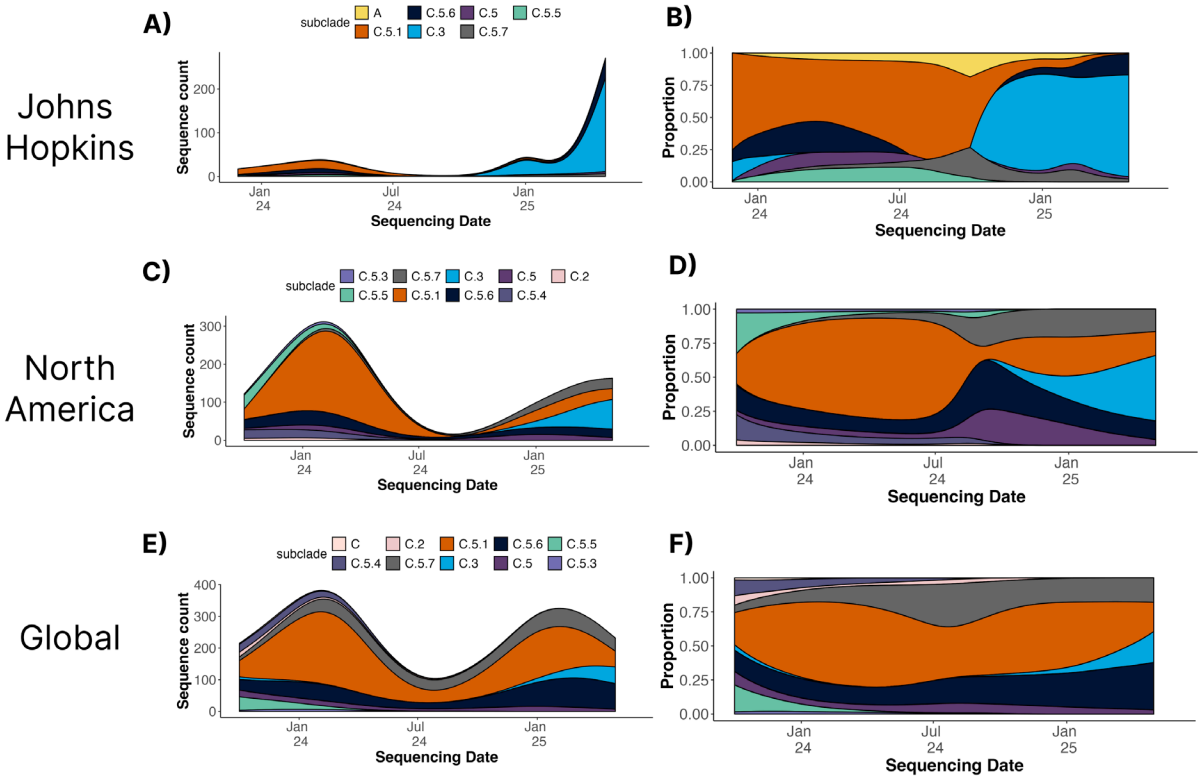

Supplemental Figure S1 – Influenza B subclade frequency between November 2024 and April 2025 within the Johns Hopkins Hospital **(A-B)** and sampled from GISAID filtered by North American origin **(C-D)** or global total **(E-F).**

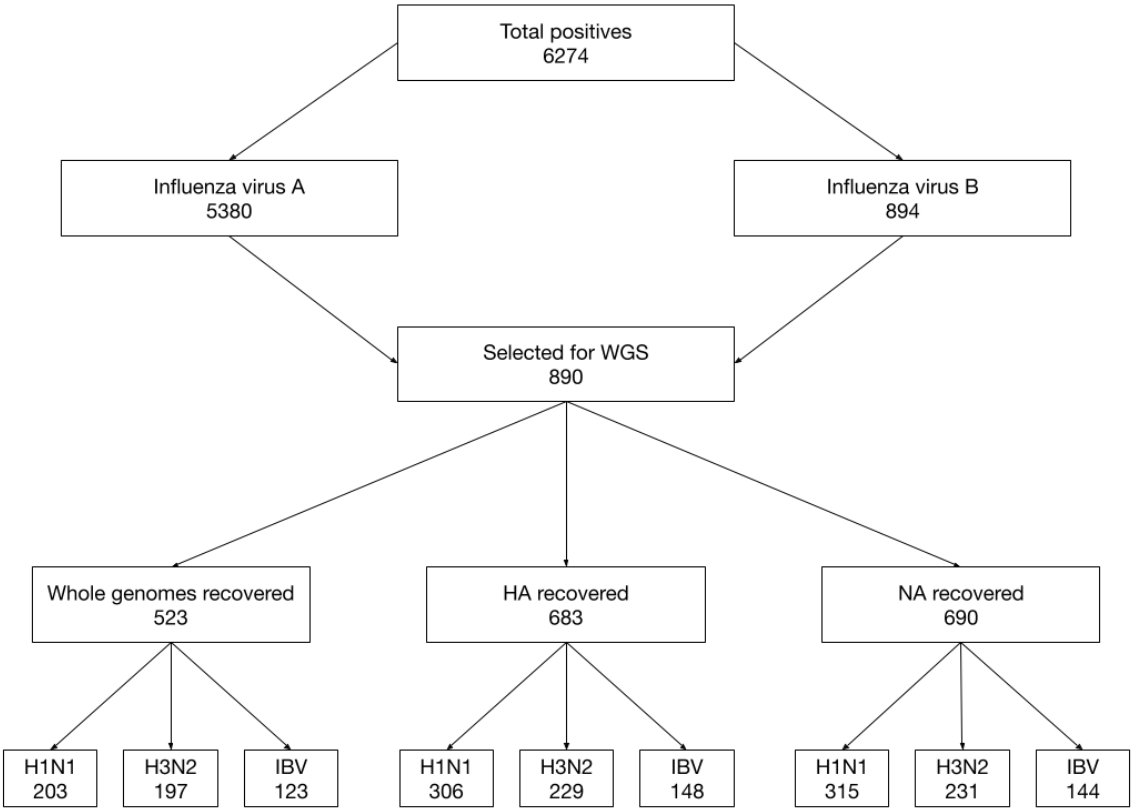

Supplemental Figure S2. Flow chart illustrating the number of samples selected for whole genome sequencing. HA and NA segments illustrates specimens where full-length HA segments were recovered.

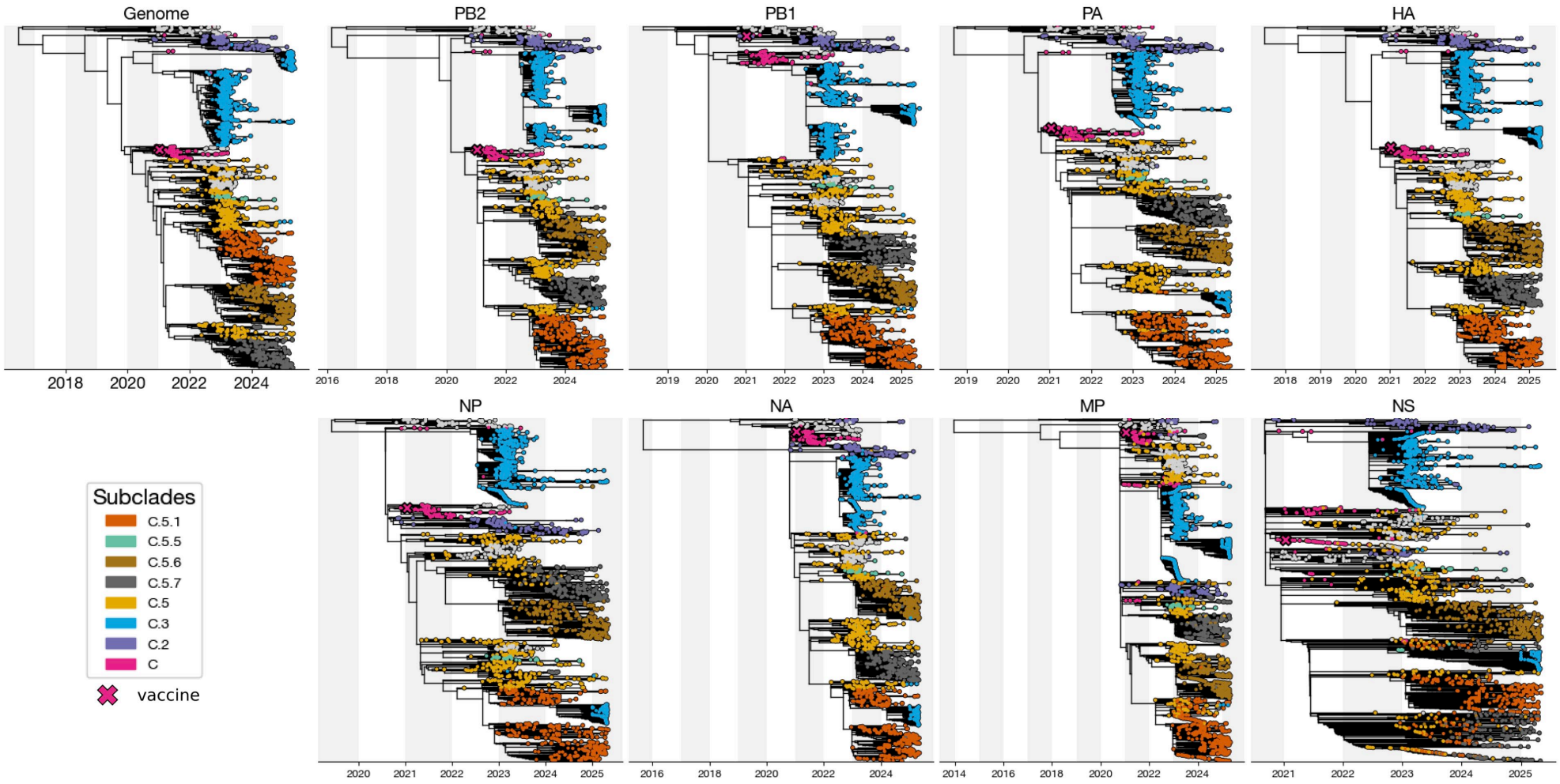

Supplemental Figure S3 – Gene tree phylogenies of the concatenated genome and 7 gene segments. The 2024-25 Influenza B vaccine component strain, B/Austria/1359417 /2021 is highlighted by an "X" on each phylogeny.

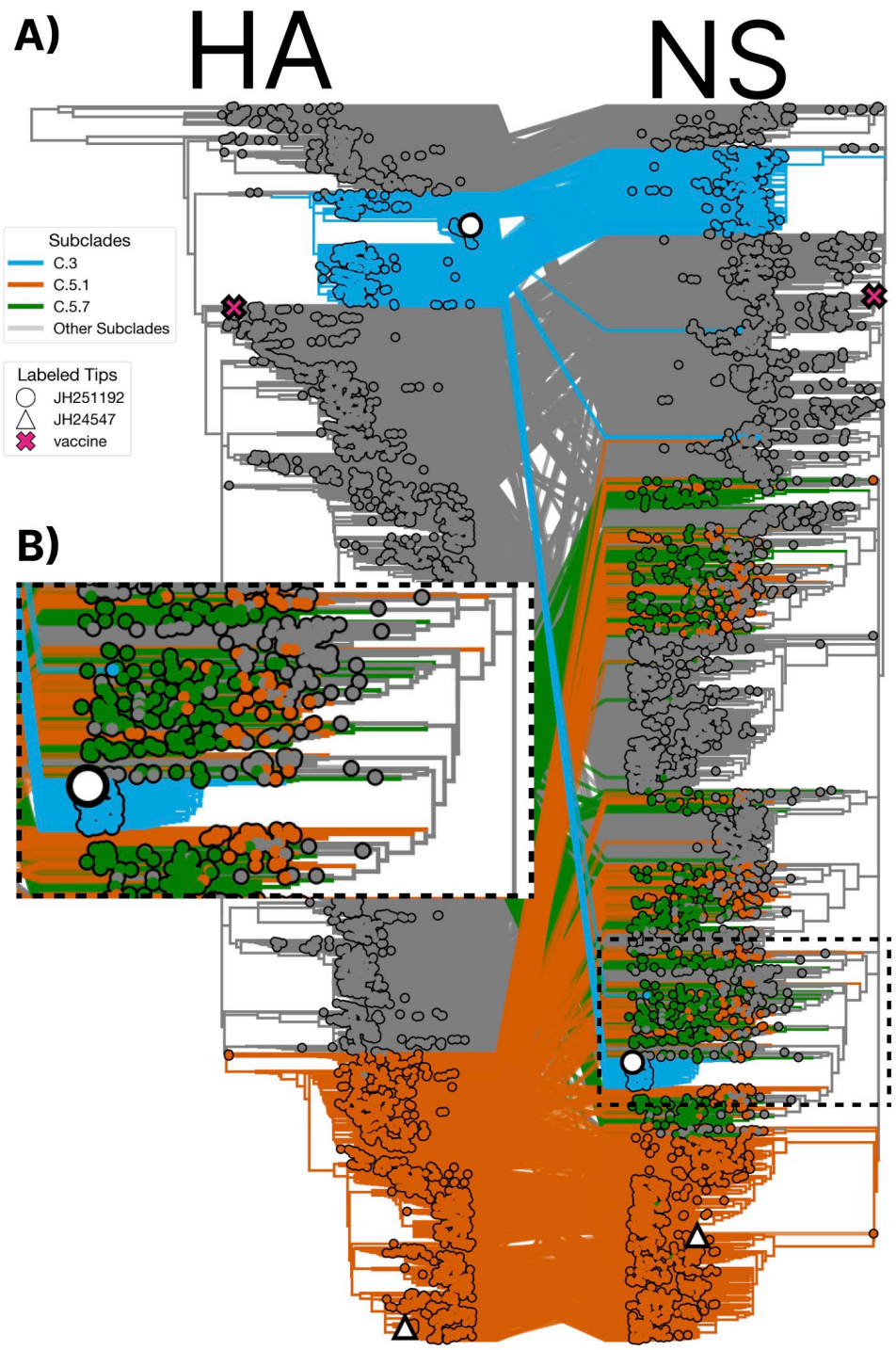

Supplemental Figure S4 – HA and NS maximum likelihood gene trees colored by C.3, C.5.6 or C.5.7 clade identity.

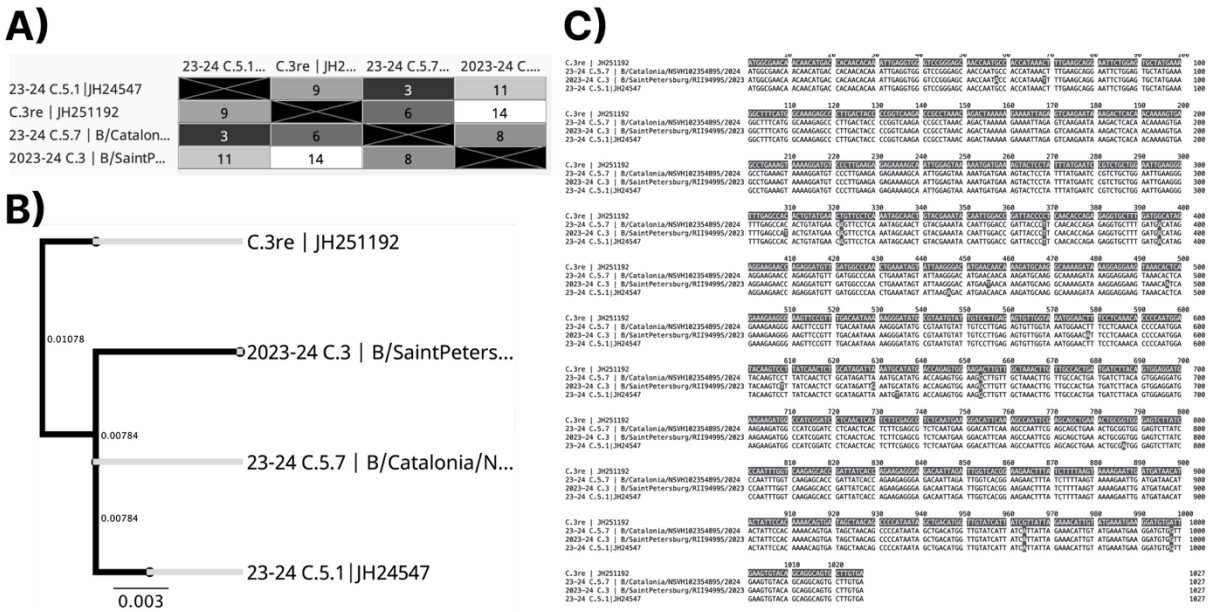

Supplemental Figure S5 – Evidence for a non-C.3 parental ancestor in reassorted C.3re strains

(A) Pairwise Differences Matrix - Number of nucleotide differences between C.3re, C.5.7, C.3 and C.5.1 subclades suggest lowest differences between subclades belongs to C.5.7. **(B)** NS gene segment nucleotide alignment with the C.3 Re subclade set as a reference (top band). **(C)** RAxML phylogenetic tree of candidate NS subclades. Dark lines represent tips and branch points; grey lines are aesthetic and connect to strain names to nodes.

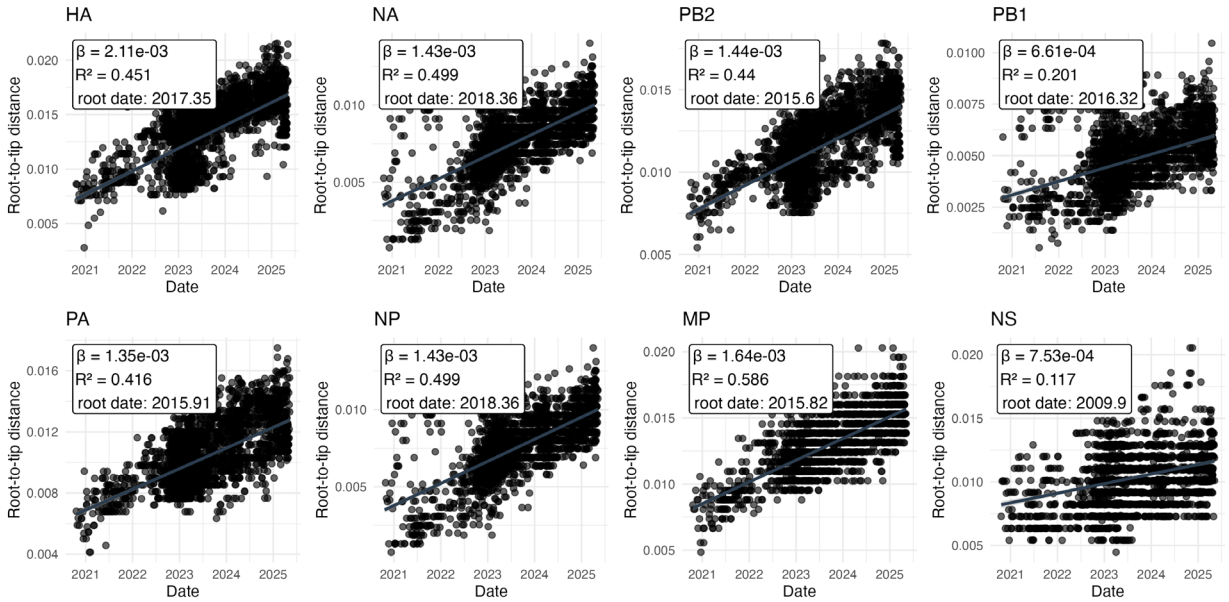

Supplemental Figure S6 – Root-to-tip regression of Influenza B segment phylogenies constructed in treetime dated to the calculated Y intercept (root date). β represents substitutions per site per year based on either collection or sequencing date.

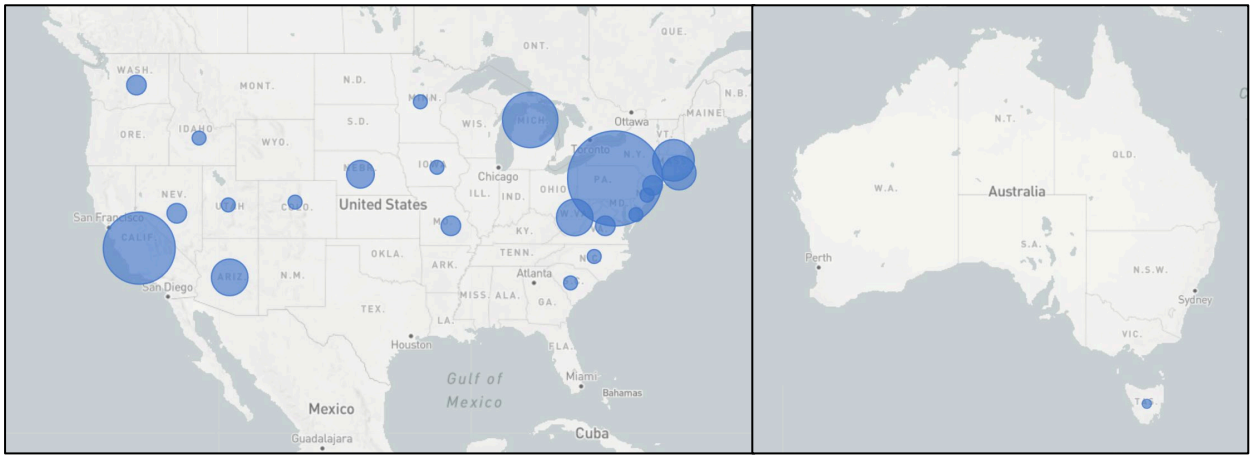

Supplemental Figure S7 – Reassortment C.3 (C.3re) lineage distribution in **(A)** North America and **(B)** Oceania as of on Jul 7, 2025. Relative size of each bubble represents the quantity of strains filtered exclusively to the C.3re 4:4 reassortment leaves. Data is interactively available at https://nextstrain.org/seasonal-flu/vic/ha/6m?c=subclade&r=division accessed on Jul 7, 2025)

Supplemental Table S1. Total Influenza case counts in the Johns Hopkins Hospital in the 2024-25 season

Date	IAV Count	IBV Count	Total Cases	IAV %	IBV %
Oct 2024	2	0	2	100.0	0.0
Nov 2024	57	4	61	93.4	6.6
Dec 2024	510	12	522	97.7	2.3
Jan 2025	1988	41	2029	98.0	2.0
Feb 2025	2229	65	2294	97.2	2.8
Mar 2025	526	372	898	58.6	41.4
Apr 2025	53	400	453	11.7	88.3
TOTAL	**5365**	**894**	**6259**	**85.7**	**14.3**

Supplemental Table S2. Clinical and demographic characteristics of patients from the Johns Hopkins Hospital using a sub-cohort of infected individuals with recoverable high-quality IBV whole genome sequences.

	Whole Cohort		C.3		C.5.X	
	count	%N	count	%N	count	%N
No. of patients	113		67		46	
Female	61	54.00%	39	58.20%	22	47.80%
Male	52	46.00%	28	41.80%	24	52.20%
Age Range						
Mean (SD)	14	13	10.8	8.94	18.6	16.2
Median	9		8		13	
Range	57		38		57	
<2	8	7.10%	4	6.00%	4	8.70%
2-5	23	20.40%	16	23.90%	7	15.20%
6-11	35	31.00%	27	40.30%	8	17.40%
12-17	17	15.00%	8	11.90%	9	19.60%
18-44	25	22.10%	12	17.90%	13	28.30%
45-55	4	3.50%	0	0.00%	4	8.70%
56-70	1	0.90%	0	0.00%	1	2.20%
Comorbidities						
Hypertension	18	15.90%	9	13.40%	9	19.60%
Lung Disease	39	34.50%	21	31.30%	18	39.10%
Kidney Disease	18	15.90%	12	17.90%	6	13.00%
Immunosupression	24	21.20%	11	16.40%	13	28.30%
Diabetes	9	8.00%	3	4.50%	6	13.00%
Heart failure	6	5.30%	2	3.00%	4	8.70%
Smoker	8	7.10%	5	7.50%	3	6.50%
Cancer	34	30.10%	23	34.30%	11	23.90%
Pregnant	1	0.90%	0	0.00%	1	2.20%
Outcome						
Admitted	20	17.70%	12	17.90%	8	17.40%
ICU	4	3.50%	2	3.00%	2	4.30%
Supplemental Oxygen	10	8.80%	4	6.00%	6	13.00%
Death	1	0.90%	0	0.00%	1	2.20%
Symptoms						
Chart count	102		59		43	
Fever	32	31.40%	21	35.60%	11	25.60%
Cough	10	9.80%	10	16.90%	4	9.30%
Headache	2	2.00%	1	1.70%	1	2.30%
Breathing problems	1	1.00%	1	1.70%	0	0.00%
Chest pain	7	6.90%	2	3.40%	5	11.60%
Sore throat	5	4.90%	3	5.10%	2	4.70%
URI	6	5.90%	4	6.80%	2	4.70%
Abdominal pain	9	8.80%	5	8.50%	4	9.30%
Emesis	7	6.90%	5	8.50%	2	4.70%
Flu-like symptoms	32	31.40%	18	30.50%	14	32.60%
Weakness	1	1.00%	1	1.70%	0	0.00%
Seizures	2	2.00%	1	1.70%	1	2.30%

Supplemental Table S3. JH-CEIRR influenza vaccine cohort age and sex study design

Age Group (years)	n (Female / Male)
21–29	10 (5 / 5)
30–39	10 (5 / 5)
40–49	10 (5 / 5)
50–59	10 (5 / 5)
60–69	10 (5 / 5)
Total	**50 (25 / 25)**

Supplemental Table S4. JH-CEIRR influenza vaccine cohort with demographics, Neutralization Titer 50% and Area Under the Curve Values (AUC) by patient.

Demographic Information				2024-25 Vaccine B/Austria/1359417/2021-Egg				B/Victoria C.5.1 B/Baltimore/JH-547/2024				B/Victoria C.3re B/Baltimore/JH-1192/2025			
				Day 0		Day 28		Day 0		Day 28		Day 0		Day 28	
Study ID	age	JH-CEIRR age grouping	sex	Reciprocal Serum NT50 Titer	AUC	Reciprocal Serum NT50 Titer	AUC	Reciprocal Serum NT50 Titer	AUC	Reciprocal Serum NT50 Titer	AUC	Reciprocal Serum NT50 Titer	AUC	Reciprocal Serum NT50 Titer	AUC
02-17-Pro-1185	63	56-70	Male	40	65	40	65	20	7.5	20	7.5	10	1.25	10	1.25
02-17-Pro-1186	68	56-70	Female	160	230	320	470	40	40	160	220	10	1.25	10	1.25
02-17-Pro-1190	25	18-44	Male	5	0.625	20	27.5	10	1.25	10	1.25	10	1.25	10	1.25
02-17-Pro-1194	47	45-55	Female	160	260	1280	1430	160	280	640	940	10	1.25	10	1.25
02-17-Pro-1198	33	18-44	Female	20	20	80	95	10	1.25	40	40	10	1.25	10	1.25
02-17-pro-1200	30	18-44	Female	20	20	640	950	10	1.25	320	1.25	10	1.25	10	1.25
02-17-Pro-1201	60	56-70	Male	160	230	640	710	80	85	80	130	10	1.25	40	1.25
02-17-pro-1203	48	45-55	Female	40	50	160	230	80	130	80	97.5	10	1.25	10	1.25
02-17-Pro-1206	25	18-44	Male	160	230	160	230	160	220	320	457.5	10	1.25	10	1.25
02-17-Pro-1208	23	18-44	Male	40	470	160	710	10	1.25	80	85	10	1.25	10	1.25
02-17-Pro-1213	36	18-44	Female	80	110	160	290	40	22.5	80	127.5	10	1.25	10	1.25
02-17-Pro-1218	36	18-44	Male	320	470	320	470	160	340	320	400	10	1.25	10	1.25
02-17-Pro-1221	31	18-44	Female	160	200	320	470	40	55	80	100	10	1.25	10	1.25
02-17-Pro-1226	31	18-44	Female	20	20	640	950	10	1.25	160	220	10	1.25	10	1.25
02-17-Pro-1228	26	18-44	Female	640	830	640	950	80	160	160	190	10	1.25	10	1.25
02-17-Pro-1231	23	18-44	Female	40	50	160	170	40	32.5	80	100	10	1.25	10	1.25
02-17-Pro-1234	29	18-44	Male	160	230	320	470	80	97.5	80	85	10	1.25	10	1.25
02-17-Pro-1236	26	18-44	Male	160	230	320	350	80	55	80	130	10	1.25	10	1.25
02-17-Pro-1241	30	18-44	Male	20	16.25	160	230	10	1.25	40	40	10	1.25	10	1.25
02-17-Pro-1249	42	18-44	Male	80	110	160	230	20	10	40	32.5	10	1.25	10	1.25
02-17-Pro-1256	44	18-44	Male	80	110	80	110	40	40	80	70	10	1.25	10	1.25
02-17-Pro-1257	49	45-55	Female	20	20	320	470	10	1.25	160	160	10	1.25	10	1.25
02-17-Pro-1259	61	56-70	Female	160	200	320	470	320	452.5	320	460	10	1.25	10	1.25
02-17-Pro-1260	28	18-44	Female	160	170	160	230	40	40	80	100	10	1.25	10	1.25
02-17-Pro-1261	42	18-44	Male	160	290	320	470	10	1.25	40	25	10	1.25	10	1.25
02-17-Pro-1262	61	56-70	Male	160	200	320	1070	320	460	640	700	20	7.5	40	32.5
02-17-Pro-1265	28	18-44	Female	40	65	80	110	320	460	640	760	10	1.25	10	1.25
02-17-Pro-1268	27	18-44	Female	10	8.75	40	65	40	40	40	80	10	1.25	10	1.25
02-17-pro-1277	50	45-55	Female	40	65	80	87.5	10	2.5	40	40	10	1.25	10	1.25
02-17-Pro-1281	63	56-70	Female	5	0.625	320	470	80	85	80	100	10	1.25	10	1.25
02-17-Pro-1285	33	18-44	Male	5	3.75	640	950	10	1.25	640	820	10	1.25	10	1.25
02-17-Pro-1290	32	18-44	Male	80	110	320	470	20	7.5	640	940	10	1.25	20	1.25
02-17-Pro-1304	43	18-44	Male	40	50	40	42.5	80	100	640	820	10	1.25	20	1.25
02-17-Pro-1305	62	56-70	Male	320	470	320	470	40	40	80	70	10	1.25	10	1.25
02-17-Pro-1307	55	45-55	Male	10	5	80	110	1280	1900	1280	2380	160	220	160	220
02-17-Pro-1308	58	56-70	Female	80	110	320	470	20	7.5	160	160	10	1.25	10	1.25
02-17-Pro-1312	38	18-44	Male	10	8.75	20	20	80	100	320	460	10	1.25	10	1.25
02-17-Pro-1313	60	56-70	Female	160	350	320	470	10	1.25	20	7.5	10	1.25	10	1.25
02-17-Pro-1314	53	45-55	Female	20	20	40	42.5	640	700	640	940	10	1.25	20	1.25
02-17-Pro-1321	49	45-55	Female	320	470	320	470	20	7.5	80	100	10	1.25	20	1.25
02-17-Pro-1323	63	56-70	Female	40	50	80	110	640	820	1280	1900	40	70	40	55
02-17-pro-1324	64	56-70	Male	80	110	160	230	80	92.5	80	112.5	10	1.25	10	1.25
02-17-pro-1331	59	56-70	Male	20	20	40	50	160	190	160	220	40	55	80	85
02-17-pro-1338	48	45-55	Female	5	1.25	160	170	20	17.5	40	55	10	1.25	10	1.25
02-17-pro-1343	51	45-55	Female	40	42.5	40	50	10	1.25	320	460	10	1.25	10	1.25
02-17-Pro-1359	50	45-55	Female	10	1.25	10	5	80	55	80	1.25	10	1.25	10	1.25
02-17-Pro-1362	48	45-55	Male	80	110	160	230	10	1.25	10	2.5	10	1.25	10	1.25
02-17-pro-1374	55	45-55	Male	5	0.625	640	950	320	415	320	460	10	1.25	10	1.25
02-17-pro-1377	57	56-70	Male	40	80	40	80	80	70	1280	1660	20	5	20	5
02-17-Pro-1378	59	56-70	Male	320	410	320	410	320	460	320	460	20	17.5	40	32.5